

A NEW GENERATION OF COOL WHITE DWARF ATMOSPHERE MODELS. III. WD J2356–209: ACCRETION OF A PLANETESIMAL WITH AN UNUSUAL COMPOSITION

S. BLOUIN¹, P. DUFOUR^{1,2}, N.F. ALLARD^{3,4}, S. SALIM⁵, R.M. RICH⁶, AND L.V.E. KOOPMANS⁷

Accepted for publication in The Astrophysical Journal

ABSTRACT

WD J2356–209 is a cool metal-polluted white dwarf whose visible spectrum is dominated by a strong and broad sodium feature. Although discovered nearly two decades ago, no detailed and realistic analysis of this star had yet been realized. In the absence of atmosphere models taking into account the nonideal high-density effects arising at the photosphere of WD J2356–209, the origin of its unique spectrum had remained nebulous. We use the cool white dwarf atmosphere code presented in the first paper of this series to finally reveal the secrets of this peculiar object and details about the planetesimal that polluted its atmosphere. Thanks to the improved input physics of our models, we find a solution that is in excellent agreement with the photometric observations and the visible spectrum. Our solution reveals that the photosphere of WD J2356–209 has a number density ratio of $\log \text{Na}/\text{Ca} = 1.0 \pm 0.2$, which is the highest ever found in a white dwarf. Since we do not know how long ago the accretion episode stopped (if it has), we cannot precisely determine the composition nor the mass of the accreted planetesimal. Nevertheless, all scenarios considered indicate that its composition is incompatible with that of chondrite-like material and that its mass was at least 10^{21} g.

Subject headings: planetary systems — stars: abundances — stars: atmospheres — stars: individual (WD J2356–209) — white dwarfs

1. INTRODUCTION

WD J2356–209⁸, was discovered by Oppenheimer et al. (2001) as part of their search for cool white dwarfs in the galactic halo. Since its spectrum shows a broad asymmetric feature around 6000 Å, it was described as having a "bizarre spectrum, incomparable to any other known object".

Using only *BRI* photometry, Bergeron (2003) attempted the first atmospheric parameter determination of WD J2356–209. It was found that it must have an effective temperature of the order of 4000 K: the best photometric solution was at $T_{\text{eff}} = 3400$ K if a hydrogen-rich atmosphere was assumed and at $T_{\text{eff}} = 4610$ K in the case of a helium-rich composition. Note that because of the absence of Balmer lines at such low temperatures, the atmospheric composition of this object remained unknown.

Shortly after, Salim et al. (2004) reobserved WD J2356–209 and confirmed the measurements of Oppenheimer et al. (2001). In particular, in a color-color dia-

gram, it appears as a strong outlier with an excessively blue $B - V$ and an extremely red $V - I$. Salim et al. (2004) suggested that these peculiar colors may be the result of a very broad Na I D doublet, implying that WD J2356–209 is a metal-polluted white dwarf (i.e., a DZ star).

Then, Bergeron et al. (2005) obtained new photometric observations of WD J2356–209 in the *BVRI* and *JH* bands. They picked up the interpretation proposed by Salim et al. (2004) and analyzed WD J2356–209 with atmosphere models that included Na. Their solution ($T_{\text{eff}} = 4790$ K and $\log \text{Na}/\text{He} = -5$) yields a satisfactory fit both to their photometric measurements and to the spectrum of Oppenheimer et al. (2001) in the 5000–9000 Å region. However, in the absence of any spectrum below 5000 Å they could not detect any other metal than Na, and thus Na and He were the only atomic species included in their atmosphere model. In retrospect, this was an unrealistic assumption. With the discovery of dozens of circumstellar debris discs around metal-polluted white dwarfs (e.g., Zuckerman & Becklin 1987; Gänsicke et al. 2006; Farihi et al. 2009; Melis et al. 2010; Rocchetto et al. 2015) and the detection of planetary transits in the light curve of WD 1145+017 (Vanderburg et al. 2015; Gänsicke et al. 2016; Croll et al. 2017) it is now clear that the presence of heavy elements in white dwarfs is the consequence of the accretion of tidally disrupted rocky bodies (Jura 2003; Farihi et al. 2010; Jura & Young 2014). Therefore, all elements representative of the composition of rocky planetesimals should be included in DZ atmosphere models.

Moreover, the analysis of Bergeron et al. (2005) was based on models that did not take into account the nonideal high-density effects that are known to arise under the physical conditions met in the atmospheres of cool white dwarfs. In particular, their models relied on

¹ Département de physique, Université de Montréal, Montréal, QC H3C 3J7, Canada; sblouin@astro.umontreal.ca, dufourpa@astro.umontreal.ca

² Institut de recherche sur les exoplanètes, Département de physique, Université de Montréal, Montréal, QC H3C 3J7, Canada

³ GEPI, Observatoire de Paris, Université PSL, CNRS, UMR 8111, 61 avenue de l'Observatoire, F-75014 Paris, France

⁴ Sorbonne Université, CNRS, UMR 7095, Institut d'Astrophysique de Paris, 98bis boulevard Arago, F-75014 Paris, France

⁵ Department of Astronomy, Indiana University, Bloomington, IN 47404, USA

⁶ Department of Physics and Astronomy, University of California, Los Angeles, CA 90095, USA

⁷ Kapteyn Astronomical Institute, University of Groningen, PO Box 800, NL-9700 AV Groningen, The Netherlands

⁸ Also known as WD 2354–211 in the electronic version of the Catalog of Spectroscopically Identified White Dwarfs (McCook & Sion 1999)

the ideal gas law, which is inappropriate for the high pressures of cool white dwarfs (e.g., Saumon et al. 1995; Becker et al. 2014); nonideal effects affecting the chemical equilibrium (Kowalski et al. 2007; Blouin et al. 2018a) were neglected; and simple Lorentzian line profiles, which poorly reproduce the spectral lines observed in cool DZ white dwarfs (Allard et al. 2016, 2018; Hollands et al. 2017), were assumed.

An independent analysis of WD J2356–209 was performed by Homeier et al. (2005, 2007) using the PHOENIX general-purpose stellar atmosphere code (Hauschildt et al. 1997; Baron & Hauschildt 1998; Hauschildt & Baron 1999) and the spectrum obtained by Oppenheimer et al. (2001). The first results identified an apparent overabundance of Na relative to Ca and suggested that WD J2356–209 has a hydrogen-rich atmosphere (Homeier et al. 2005). An important limitation of this first analysis was that line profiles implemented in their atmosphere models were limited to perturber densities not exceeding 10^{19} cm^{-3} (Allard et al. 2003), which is about three orders of magnitude below the density at the photosphere of a $T_{\text{eff}} = 4000 \text{ K}$ helium-rich DZ white dwarf (Blouin et al. 2018a). In a second analysis (Homeier et al. 2007), improved line profiles appropriate for larger densities were employed and a helium-rich composition was favored. Homeier et al. (2005, 2007) were also the first to point out that metal hydrides (namely, MgH and CaH) should form under the conditions encountered in the atmosphere of WD J2356–209. However, these preliminary analyses were exploratory in nature and no quantitative fit to the spectroscopic and photometric data was attempted. Furthermore, as in Bergeron et al. (2005), their models did not include the nonideal effects that are known to affect the chemical equilibrium and the equation of state.

In this paper, the third of a series, we present the most detailed analysis to date of WD J2356–209. Our models, which include an accurate description of the high-pressure physics relevant to the modeling of cool DZ stars (see Blouin et al. 2018a,b, hereafter Papers I and II), make it possible for the first time to obtain a satisfactory fit to the photometric data and to the entire visible spectrum. In Section 2, we present the observations on which our analysis of WD J2356–209 is based. A few new improvements brought to our model atmosphere code are detailed in Section 3. Section 4 contains our analysis of WD J2356–209, where we find that the sodium to calcium ratio is the highest ever encountered in a white dwarf photosphere. Finally, Section 5 provides a discussion on the origins of the peculiar abundances measured in WD J2356–209 and our conclusions are given in Section 6.

2. OBSERVATIONS

Our analysis of WD J2356–209 makes use of *BVRI* and *JH* photometry from Bergeron et al. (2005), *grizy* photometry from Pan-STARRS (Chambers et al. 2016) and the *Gaia* DR2 parallax measurement (Gaia Collaboration 2016, 2018). The parallax indicates that WD J2356–209 is located at a distance $D = (64.8 \pm 2.5) \text{ pc}$ from the Earth, which is in good agreement with the estimation obtained by Salim et al. (2004) using color-magnitude relations ($74 \pm 34 \text{ pc}$).

For the spectroscopy, we rely on data obtained with

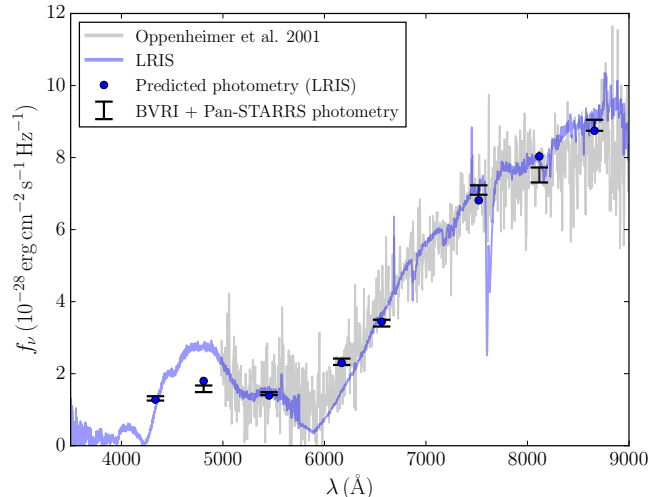


FIG. 1.— Observed spectra and photometry of WD J2356–209. The spectrum of Oppenheimer et al. (2001) is in gray and the Keck LRIS spectrum is in blue. Note that the LRIS spectrum was scaled so that the predicted photometry (blue circles) match the observed photometry (black error bars).

LRIS (Oke et al. 1995) on Keck I telescope on 2002 September 14. A 300/5000 grating was used for both the blue and the red spectra, together with a 1 arcsec slit, giving an effective resolution of 10.3 \AA . D560 dichroic was used to split the beams, giving useful wavelength coverage of 5000–9000 \AA on the red side and 3500–5800 \AA on the blue side. Each of the blue and red spectra were obtained with a total exposure time of 45 minutes. Standard arc spectra were taken for wavelength calibration. Only one standard star was available for flux calibration, while there were no suitable observations for the removal of the telluric absorption. The observations of the standard star may have been affected by detector non-linearity. Therefore, we correct the flux calibration by scaling the spectrum so that the photometry extracted from the joined blue/red spectrum agrees with the broadband photometry. As shown in Figure 1, the scaled LRIS spectrum agrees very well with the low-resolution shallow spectrum of Oppenheimer et al. (2001) in the region where they overlap ($> 5000 \text{ \AA}$).

3. ATMOSPHERE MODELS

The atmosphere models used in this work are described at length in Paper I. Our models are uniquely suited for the analysis of such a very cool DZ star, since they are the only ones to include both a state-of-the-art description of the ionization equilibrium of heavy elements (Paper I) and unified line profiles (Allard et al. 1999) for the strong Na and Ca spectral lines that characterize the spectrum of WD J2356–209.

Compared to the models used in Papers I and II, two changes were made to our code. First, we have improved our collisional profiles of the resonance line of neutral calcium perturbed by helium using the ab initio Ca–He potential energies of M. Krośnicki reported in Hernando et al. (2008). It is a significant improvement in the description of Ca–He singlet potential energies, but only at close range (i.e., only for radiator-perturber separations of ≈ 3.5 to 11 \AA). To predict the impact core shift and width, the long-range part of the potential energies needs

to be accurately determined. Moreover, our approach requires prior knowledge of the variation of the radiative dipole moments with atom-atom separation for each molecular state. As this variation is unknown at present, the dipole moments were assumed to remain constant throughout the collision. In order to obtain more accurate line profiles, intensive ab initio calculations are being performed to obtain both the ground and first excited potential energy curves (PECs) and the transition dipole moments for the Ca–He system (N. F. Allard et al., in preparation).

The second change made to our atmosphere model code was to add the opacity due to the rovibrational transitions of the MgH and CaH molecules. The MgH opacities are computed using the linelists of GharibNezhad et al. (2013) for the the $X^2\Sigma^+ \rightarrow A^2\Pi$ and $X^2\Sigma^+ \rightarrow B^2\Sigma^+$ transitions, which are available on the ExoMol website⁹ (Tennyson & Yurchenko 2012; Tennyson et al. 2016). For CaH, the $X^2\Sigma^+ \rightarrow A^2\Pi$ and $X^2\Sigma^+ \rightarrow B^2\Sigma^+$ transitions are computed using the Kurucz linelists¹⁰, which rely on molecular data from Weck et al. (2003) and Shayesteh et al. (2013).

4. ANALYSIS OF WD J2356–209

We rely on the *BVRIJH* and *grizy* photometry of WD J2356–209 to find its effective temperature, surface gravity and H/He abundance ratio. More specifically, the solid angle $\pi(R/D)^2$ and T_{eff} are found by fitting the model fluxes to the spectral energy distribution. Since the distance D is already known from the *Gaia* parallax, we can obtain the radius R from the solid angle. The mass of the white dwarf (and the corresponding surface gravity) are then found using the evolutionary models of Fontaine et al. (2001) with C/O cores, $\log(M_{\text{He}}/M_{\star}) = -2$ and $\log(M_{\text{H}}/M_{\star}) = -10$, which are representative of helium-atmosphere white dwarfs. The H/He abundance ratio is inferred from the infrared photometric measurements, which are affected by the presence of H_2 –He collision-induced absorption (CIA, Jørgensen et al. 2000; Blouin et al. 2017). Once a photometric solution is found, we use the spectroscopic data to constrain the abundances of Na, Ca, Fe and Mg. In particular, the Na I D doublet is used to derive the Na/He ratio, the Ca I 4226 Å and Ca II H & K lines for Ca/He, Fe I and Fe II lines in the 3600–3800 Å region for Fe/He, and the MgH rovibrational bands between 5000 and 5300 Å for Mg/He. Once the heavy element abundance ratios are found, the whole fitting procedure – including the photometric fit – is repeated until internal consistency is reached.

Figure 2 compares our best solution to the photometric and spectroscopic data. Except for the core of the Na I D doublet and an unknown feature near 4500 Å, our fit is in excellent agreement with the observations across all wavelengths. In particular, our spectroscopic fit closely matches the Fe lines at small wavelengths, the Ca II H & K and Ca I 4226 Å lines, the blue and red wings of the Na I D doublet, and the flux depletion between 5000 and 5500 Å. Note that due to strong telluric absorption we could not use the Na I doublet at 8200 Å to validate

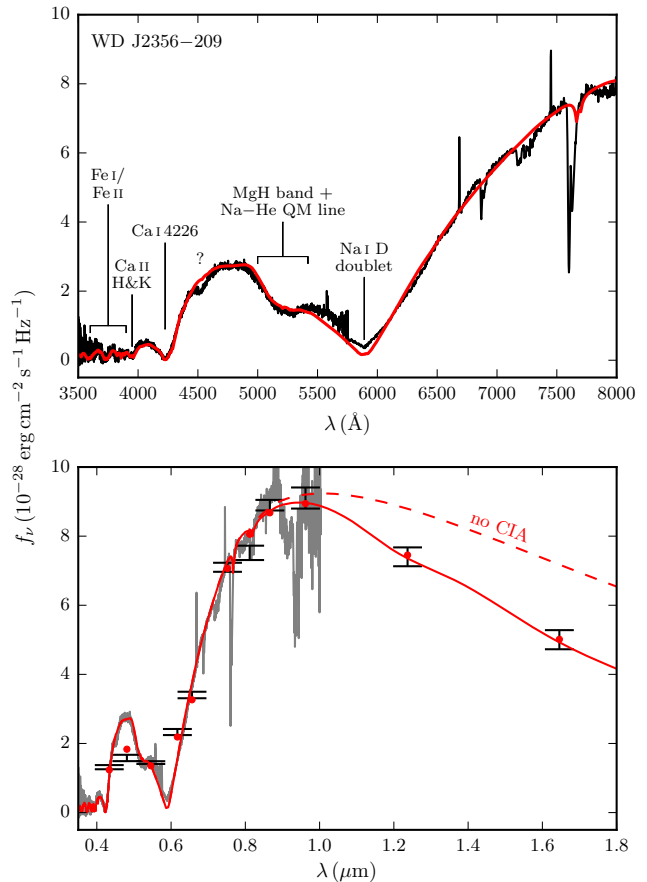


FIG. 2.— Our best solution for WD J2356–209. The top panel shows our fit (in red) to the visible spectrum (in black) and the bottom panel shows our photometric fit to the *BVRI*, *JH* and *grizy* bands (the photometric observations are represented by the error bars). The dashed spectrum in the bottom panel was computed from our best-fitting model, but without including H_2 –He CIA in the synthetic spectrum calculation. The strong absorption lines near 7600 Å are of telluric origin and were ignored in our analysis.

the sodium abundance inferred from the Na I D doublet. Regarding the photometric fit, we found that a mix H/He atmosphere has to be assumed to produce the H_2 –He CIA that is required to properly match the *J* and *H* bands.

The atmospheric parameters of WD J2356–209 are given in Table 1. Its very cool temperature of $T_{\text{eff}} = 4040 \pm 110$ K makes it – to our knowledge – the oldest known DZ star, with a cooling age of 8.0 ± 0.8 Gyr.¹¹

Table 1 also lists the constraints on metal abundance ratios in the atmosphere of WD J2356–209. Apart from the sodium abundance, which is further discussed in Section 5, all abundances are close to the average values measured in metal-polluted atmospheres. In particular, in a ternary diagram of Ca, Mg and Fe abundances (e.g., Hollands et al. 2018, Figure 2), WD J2356–209 would be

¹¹ Note that Giammichele et al. (2012) found a greater cooling age (8.5 Gyr) for WD 2251–070. However, their analysis was based on a model atmosphere code (Dufour et al. 2007) that did not include a detailed description of the high-density effects arising at the photosphere of such a cool object. Our reanalysis of WD 2251–070 (Section 4.3) suggests that it has an effective temperature $T_{\text{eff}} = 4050 \pm 60$ K and a surface gravity $\log g = 7.94 \pm 0.04$, which corresponds to a cooling age of 7.5 ± 0.5 Gyr.

⁹ <http://exomol.com>

¹⁰ <http://kurucz.harvard.edu>

TABLE 1
WD J2356–209 ATMOSPHERIC
PARAMETERS

Parameter	Value
T_{eff}	4040 ± 110 K
$\log g$	7.98 ± 0.07
$\log \text{H}/\text{He}^{\text{a}}$	-1.5 ± 0.2
$\log \text{C}/\text{He}$	< -6.0
$\log \text{O}/\text{He}$	$(< -4)^{\text{b}}$
$\log \text{Na}/\text{He}$	-8.3 ± 0.2
$\log \text{Mg}/\text{He}$	-8.0 ± 0.2
$\log \text{Al}/\text{He}$	< -8.8
$\log \text{Si}/\text{He}$	(< -6.8)
$\log \text{K}/\text{He}$	< -10.0
$\log \text{Ca}/\text{He}$	-9.3 ± 0.1
$\log \text{Ti}/\text{He}$	< -9.8
$\log \text{Cr}/\text{He}$	< -9.9
$\log \text{Mn}/\text{He}$	< -10.7
$\log \text{Fe}/\text{He}$	-8.6 ± 0.2
$\log \text{Ni}/\text{He}$	< -8.0

^a All abundances are reported as ratios of number densities

^b The abundances in parentheses are not firm limits (see text)

close to the bulk of DZ stars. The constraints on Al, K, Ti, Cr, Mn and Ni, for which no feature is observed in the spectrum of WD J2356–209, were found by raising their abundances up to the point where a spectral line should be visible. Note that the constraint on the K/He ratio was found using the spectrum of Oppenheimer et al. (2001) instead of the LRIS spectrum, since the latter shows strong telluric features near the K I 7665/7699 Å lines (see Figure 1). The constraint on C/He was established using the C₂ rovibrational bands instead of the atomic carbon lines, since the former require a smaller carbon abundance before being visible in the spectrum. Finally, no firm constraints could be found for the abundances of O and Si, since even the addition of a very large amount of these elements does not result in any visible spectral lines. The limits for O/He and Si/He given in Table 1 are therefore lower-bound estimates of the maximum abundance of these elements that is compatible with the spectroscopic observations of WD J2356–209.

Our excellent fit to the wings of the broad Ca and Na spectral lines of WD J2356–209 (Figure 2) was made possible thanks to the improved lines profiles implemented in our models (Allard & Alekseev 2014; Allard et al. 2014). This good agreement indicates that our model predicts the right physical conditions in the line-forming regions of the atmosphere. In particular, it suggests that the total number density n_{tot} is accurate, since it is the parameter that governs the broadening of the spectral lines. At the photosphere of WD J2356–209, the pressure is high enough ($\log P = 10.0$) that deviations from the ideal gas law begin to be important (see Figure 4 of Paper I). If the ideal gas law was assumed, n_{tot} would be 20% higher and the line profiles would be slightly broader (particularly the Na I D doublet). Note though that WD J2356–209 cannot be used to validate our implementation of pressure ionization, since its photospheric density ($\rho = 0.1 \text{ g cm}^{-3}$) is too small to induce significant deviations from the ideal Saha equation (Kowalski et al. 2007, Paper I).

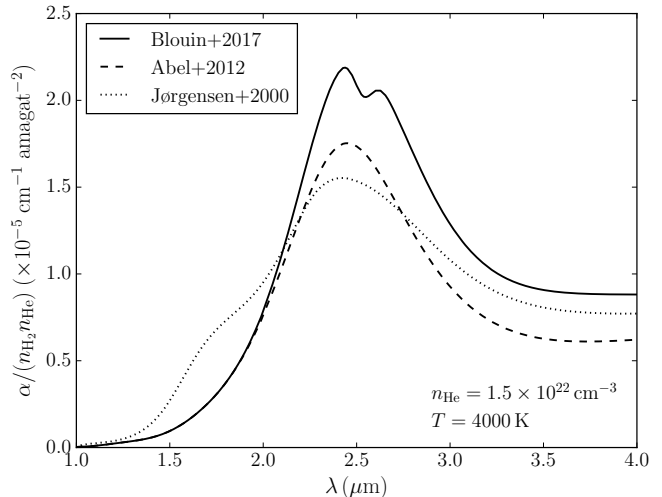


FIG. 3.— H₂–He CIA profiles at 4000 K and $n_{\text{He}} = 1.5 \times 10^{22} \text{ cm}^{-3}$, as computed by Blouin et al. (2017, Equation 7), Abel et al. (2012) and Jørgensen et al. (2000). The absorption profiles are divided by the number density of H₂ and He and are therefore constant with respect to density (with the exception of the Blouin et al. profile, which includes the effects of many-body collisions).

4.1. Collision-induced absorption

Figure 3 compares the H₂–He CIA profiles obtained by different authors for physical conditions that are representative of the photosphere of WD J2356–209. Differences between the profiles imply that the H/He ratio derived from the photometry depends on the choice of the CIA profiles implemented in our models. In particular, if the profiles of Jørgensen et al. (2000) were assumed, a smaller hydrogen abundance would be found. In fact, as already noted in Paper II, the profiles of Jørgensen et al. (2000) predict a too strong absorption in the $\approx 1.2 - 2 \mu\text{m}$ region, possibly because the potential energy and induced dipole surfaces used to derive those profiles were computed with a smaller atomic orbital basis set.

Furthermore, Figure 3 shows that significant differences between the profiles of Abel et al. (2012) and Blouin et al. (2017) appear above $2 \mu\text{m}$ (particularly near the maximum of the fundamental band at $\approx 2.5 \mu\text{m}$). Those differences are due to many-body collisions (which are only included in the profiles of Blouin et al.) that lead to an enhancement and a distortion of the absorption profile. The only photometric measurements available beyond the *H* band are those from the Wide-field Infrared Survey Explorer (WISE, Wright et al. 2010) for the 3.4 and 4.6 μm bands. Our best fit is compatible with those measurements, but their large uncertainties do not allow us to explicitly confirm that the CIA is indeed enhanced by many-body effects.

4.2. The Na–He satellite and the MgH bands

The wide absorption feature in the blue wing of the Na I D doublet proved particularly challenging to model. Allard et al. (2014) suggested that it could be the result of the quasi-molecular satellite feature arising from the Na–He interaction. Our detailed analysis reveals that it is only part of the explanation and that MgH rovibrational bands must be included to fully explain this absorption feature. Figure 4 compares our best fit to

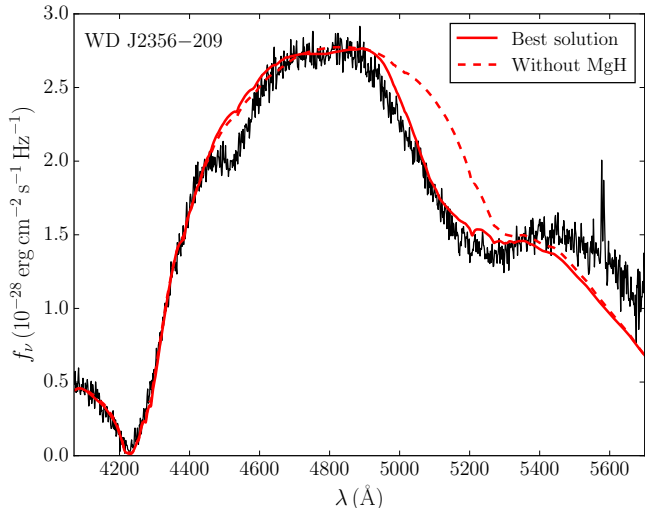


FIG. 4.— Comparison between the best solutions found when including (solid line) and when omitting (dashed line) the MgH bands in our models.

the 5000–5500 Å absorption feature with and without the MgH bands. Clearly, the Na–He satellite visible in the fit that omits the MgH bands (dashed line) is not sufficient to explain the whole absorption feature and MgH absorption bands must be invoked.

We emphasize that including MgH in our models is physically motivated. Given the temperature of WD J2356–209, its hydrogen abundance (independently constrained from the H₂–He CIA) and the presence of magnesium (which is given by a Mg/Ca ratio that is very close to the value expected for chondrite-type material), MgH has to be present at the photosphere of WD J2356–209. To our knowledge, this is the first detection of MgH molecular features in a white dwarf. MgH bands were proposed by Dufour et al. (2006) to explain the asymmetry of the Mg I 5175 Å line in G165–7, but it was later shown that improved line profiles – beyond the impact approximation – are enough to explain this asymmetry (Allard et al. 2016). Finally, note that for our derived atmospheric parameters CaH is not sufficiently abundant to produce visible bands around 7000 Å.

4.3. The unknown absorption feature near 4500 Å

Our fit of WD J2356–209 does not reproduce the small asymmetric absorption feature near 4500 Å (Figure 4). Technically, boosting the Ti/Ca ratio by a factor of ≈ 10 with respect to chondritic abundances allows the Ti I $a^5F - y^5F^\circ$ multiplet (centered at 4535 Å) to be strong enough to reasonably match the absorption feature near 4500 Å. However, another cool DZ star, WD 2251–070, offers good reasons to be suspicious of this interpretation.

Indeed, WD 2251–070 also shows a strikingly similar absorption feature in that region (Figure 5). Using photometric and spectroscopic data reported in Bergeron et al. (1997) and Dufour et al. (2007), we analyzed WD 2251–070 with our cool DZ grid. Our preliminary fit yields $T_{\text{eff}} = 4050 \pm 60$ K, $\log g = 7.94 \pm 0.04$, $\log \text{H}/\text{He} < -4.5$, $\log \text{Na}/\text{He} < -10.3$ and $\log \text{Ca}/\text{He} = -10.0 \pm 0.1$ (an in-depth analysis of this object will be presented in N. F. Allard et al., in preparation). Given the strong similarities between WD 2251–070 and WD J2356–209

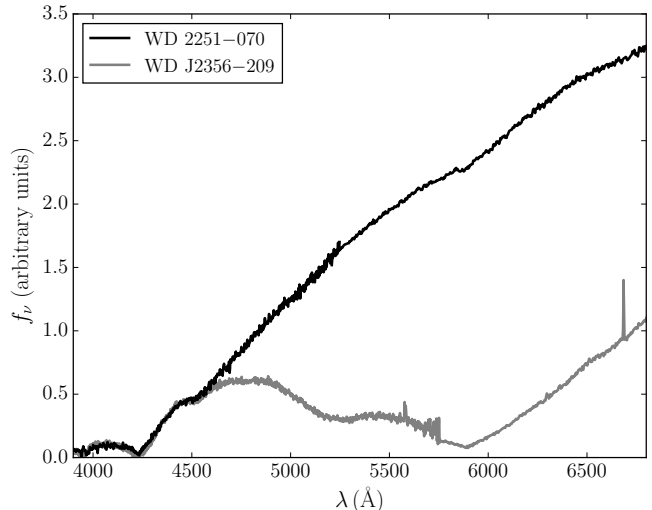


FIG. 5.— Comparison of the spectrum of WD J2356–209 to that of WD 2251–070. The data for WD 2251–070 is from Bergeron et al. (1997) and Dufour et al. (2007). Note the resemblance between both spectra below 4600 Å and their strong dissimilarity at longer wavelengths.

(i.e., same feature near 4500 Å, similar Ca abundances and virtually identical effective temperatures), it is very likely that the origins of the 4500 Å absorption feature are the same for both objects. If it is the case, then there is a good reason to reject Ti as the explanation for this feature. Boosting the Ti ratio to produce a sufficiently strong Ti I $a^5F - y^5F^\circ$ multiplet also implies that the similarly important $a^5F - y^5G^\circ$ multiplet (centered around 5020 Å) should be visible. By adjusting the Mg abundance, our fit of WD J2356–209 could accommodate the additional opacity resulting from the Ti I $a^5F - y^5G^\circ$ multiplet. However, the spectrum of WD 2251–070 clearly rules out the presence of any absorption feature around 5020 Å and thus suggests that Ti cannot be the explanation of the 4500 Å absorption feature.

Still, since we rely on Lorentzian line profiles for all Ti spectral lines, we need to be careful before completely ruling out Ti as the source of the 4500 Å feature. In principle, it is possible that accurate line profile calculations will show that the $a^5F - y^5G^\circ$ multiplet is flattened out under the density conditions encountered at the photosphere of WD 2251–070 ($n_{\text{He}} \approx 6 \times 10^{22} \text{ cm}^{-3}$). However, there is a second argument against the Ti scenario. We constrained the Na abundance in WD 2251–070 to $\log \text{Na}/\text{He} < -10.3$, implying that it has a $\log \text{Na}/\text{Ca}$ ratio smaller than -0.3 . This ratio is vastly different from the $\log \text{Na}/\text{Ca} = 1.0$ ratio found for WD J2356–209 and we therefore expect the abundance pattern of WD 2251–070 to be quite different from that of WD J2356–209. In particular, it would be surprising if WD 2251–070 and WD J2356–209 had similar Ti/Ca ratios but significantly different Na/Ca ratios. All things considered, it is unlikely that the feature near 4500 Å is due to Ti.

Alternatively, since it is observed in two white dwarfs with similar Ca abundances, it is tempting to explain the 4500 Å feature as being due to Ca. In a dense helium medium, it turns out that the Ca II H & K profile can

show a quasi-molecular feature near 4500 Å (Allard & Alekseev 2014). However, for the physical conditions in the atmosphere of WD 2251–070 and WD J2356–209, this quasi-molecular line is predicted to be too weak to explain the shape of the spectrum around 4500 Å. We are therefore unable to identify the origin of this feature at the moment.

5. HOW TO EXPLAIN THE HIGH SODIUM ABUNDANCE?

As it is well above the chondritic value of $\log \text{Na}/\text{Ca} = 0.0$ (Lodders 2003), the $\log \text{Na}/\text{Ca} = 1.0 \pm 0.2$ ratio measured in WD J2356–209 is surprising and needs to be explained. Note that this extreme abundance ratio is not only supported by our excellent fit to the observations (Figure 2), but also by the direct comparison of WD J2356–209 to WD 2251–070. While both objects have a very similar calcium abundance and a virtually identical effective temperature, their spectra are drastically different in the region affected by the Na I D doublet (as seen in Figure 5).

5.1. Comparison to other sodium-rich stars

WD J2356–209 is not the only white dwarf to have a high Na/Ca abundance ratio. A few objects with $\log \text{Na}/\text{Ca} > 0$ were identified by Hollands et al. (2017) and are shown in Figure 6. However, because of the very noisy spectra of many of those objects, the derived abundances are often highly uncertain. Using our own atmosphere model grid, we performed a reanalysis of this sample and we found that, within the uncertainties, most of those objects are compatible with a chondritic abundance ratio of $\log \text{Na}/\text{Ca} = 0$ (a detailed analysis will be presented in S. Coutu et al., in preparation). In fact, we found compelling evidence of a high Na/Ca abundance ratio only for three objects (SDSS J095645.14+591240.6, SDSS J164939.23+223807.2 and SDSS J212312.20+001653.5). Another potentially sodium-rich white dwarf, G77–50, was analyzed by Farihi et al. (2011). They found a $\log \text{Na}/\text{Ca} = 0.7$ abundance ratio, but this result should also be taken with a grain of salt as the magnetism of this object complicates its analysis and the authors explicitly noted that their sodium abundance measurement is uncertain.

Furthermore, Harris et al. (2003) identified a faint ($g = 21.4$) DZ star in the Sloan Digital Sky Survey (SDSS) that has a spectrum that also appears to show a broad Na line. As WD J2356–209, the visible spectrum of SDSS J133001.13+643523.7 (J1330+6435) is dominated by a strong and broad Na I D doublet. Figure 7 shows our best solution for this star and Table 2 lists its derived atmospheric parameters. Note that a hydrogen-free atmosphere was assumed, since we do not have any infrared photometry to fit the H/He ratio to an eventual infrared flux depletion.¹² The SDSS spectrum being noisy, the Ca/He and Na/He abundance ratios are subject to considerable uncertainties. Nonetheless, it is clear that the Na/Ca ratio of J1330+6435 is higher than average, but well below the extreme ratio found

¹² In any case, the addition of a moderate amount of hydrogen (up to $\log \text{H}/\text{He} = -1.5$) does not change our conclusions on the Na/Ca abundance ratio of this object.

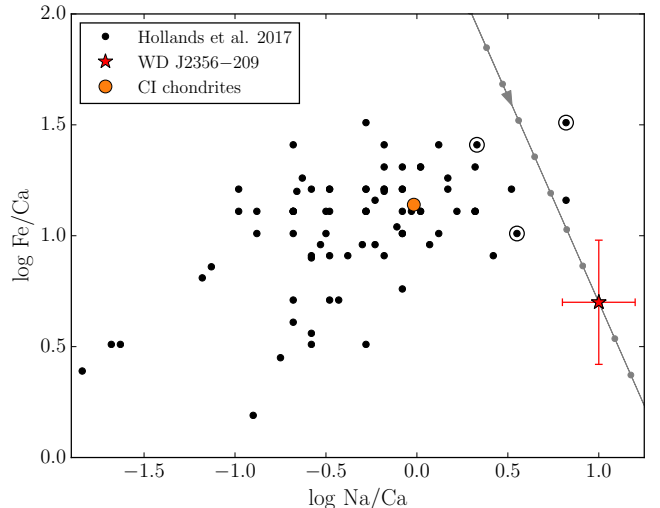


FIG. 6.— Elemental abundances for CI chondrites (Lodders 2003, filled orange circle), WD J2356–209 (red star) and the DZ stars analyzed by Hollands et al. (2017, filled black circles). The three encircled objects are those for which we found compelling evidence of a Na/Ca abundance ratio greater than 1. Note that magnetic objects in the Hollands et al. (2017) sample are not shown in this figure. The gray line indicates how the metal abundances in WD J2356–209 would have evolved, assuming the diffusion timescales mentioned in the text. The distance between two gray circles on the chemical evolution track corresponds to 1 Myr.

TABLE 2
J1330+6435 ATMOSPHERIC PARAMETERS

Parameter	Value
T_{eff}	$4310 \pm 190 \text{ K}$
$\log g$	8.26 ± 0.15
H/He	0
$\log \text{Na}/\text{He}$	-8.5 ± 0.3
$\log \text{Ca}/\text{He}$	-8.8 ± 0.3

for WD J2356–209. While there are some objects with a Na/Ca abundance ratio above the chondritic value, WD J2356–209 is the most extreme case ever encountered.

5.2. Constraints on the accreted planetesimal

The abundances of heavy elements in a DZ star are indicative of the nature of the accreted parent body and can be used to infer its composition (Zuckerman et al. 2007; Koester et al. 2011; Dufour et al. 2012; Hollands et al. 2018; Harrison et al. 2018). Such studies have highlighted the existence of a great diversity of accreted bodies, ranging from Kuiper-Belt-Object analogs (Xu et al. 2017) to differentiated rocky bodies (Zuckerman et al. 2011; Melis & Dufour 2017) and water-bearing planetesimals (Farihi et al. 2013; Raddi et al. 2015). Can we relate the high Na/Ca ratio of WD J2356–209 to any solar system counterpart?

Table 3 lists the Na/Ca ratio of a few solar system objects. The only measurements compatible with the composition of WD J2356–209 are those obtained for the dust of the comet 67P/Churyumov-Gerasimenko (67P). Those measurements were obtained by the COmetary Secondary Ion Mass Analyzer (COSIMA, Kissel et al. 2007) onboard the *Rosetta* spacecraft while it followed

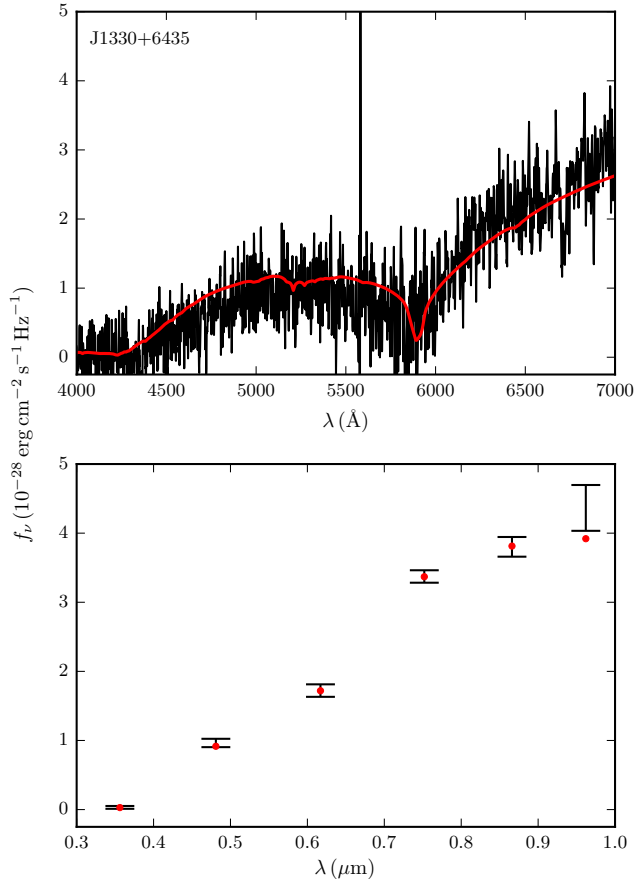


FIG. 7.— Our best solution for J1330+6435. The top panel shows our fit to the visible spectrum and the bottom panel displays our photometric fit to the SDSS *u* band and Pan-STARRS *grizy* bands. Note that the SDSS spectrum was smoothed for clarity.

TABLE 3
SODIUM ABUNDANCES

Object	$\log \text{Na}/\text{Ca}^a$	Reference
WD J2356–209	1.0 ± 0.2	This paper
CI chondrites	-0.017 ± 0.002	Lodders (2003)
Bulk Earth	-0.64 ± 0.04	Wang et al. (2018)
Earth’s mantle	-0.74 ± 0.04	Wang et al. (2018)
Earth’s crust	0.00	Rumble (2018)
Halley	0.2 ± 0.3	Jessberger et al. (1988)
67P	1.2 ± 0.6	Bardyn et al. (2017)

^a Ratio of number densities

comet 67P at close distances for two years. Additionally, with the exception of Mn and Fe, the abundances of the other heavy elements in WD J2356–209 are compatible with those measured in the dust of comet 67P (Figure 8).

That being said, the total mass accreted by WD J2356–209 is incompatible with the mass of a comet. By estimating the mass of metals currently in the convection zone, we can obtain a lower limit on the total accreted mass (it is a lower limit since diffusion might already have evacuated heavy elements from the convection zone). Using the envelope model code of Rolland et al. (2018), we find that the fractional mass of the convection zone is $\log q = -5.49$ for a $T_{\text{eff}} = 4000$ K

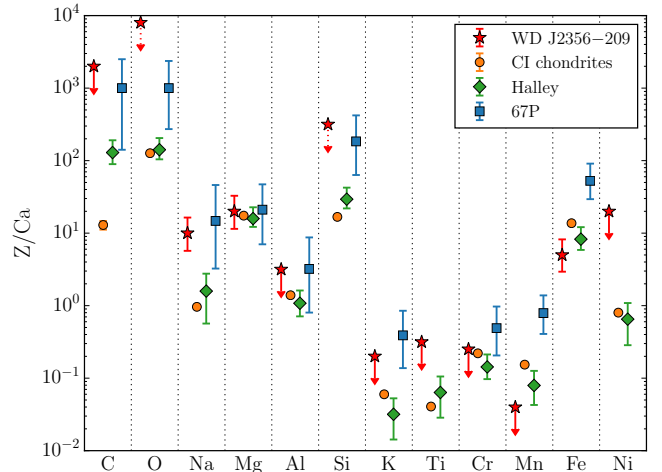


FIG. 8.— Elemental abundances by number relative to Ca. The data for WD J2356–209 is from Table 1, chondritic abundances are taken from Lodders (2003) and the data for comets Halley and 67P are from Jessberger et al. (1988) and Bardyn et al. (2017), respectively. The upper limits represented by dotted arrows are those for which no firm constraint could be established. Note that the abundances for WD J2356–209 correspond to the abundance ratios of the accreted planetesimal only if accretion is in its early phase (i.e., the effects of relative diffusion are not included in this figure).

white dwarf with $\log g = 8$ and $\log \text{H}/\text{He} = -1.5$. With this value, we find that the total mass in the convection zone of the four heavy elements clearly detected in WD J2356–209 (Ca, Mg, Na and Fe) is 5×10^{20} g. This value could significantly underestimate the total mass of metals currently in the convection zone, since it does not include C, O and Si, three elements that are expected to be particularly abundant (Figure 8). A higher estimate can be obtained by assuming that the accreted planetesimal had a chondritic composition relative to Ca and computing its total mass from the abundance of Ca detected in WD J2356–209. Using the values published in Lodders (2003), this yields a mass of $\sim 10^{21}$ g. This mass is significantly higher than the mass of comet 67P (10^{16} g, Pätzold et al. 2016) and that of the most massive comets of the solar system (Hale-Bopp has a mass of $\sim 10^{19}$ g, Weissman 2007), suggesting that a single comet cannot be the cause of the pollution of the atmosphere of WD J2356–209. As the lower limit on the accreted mass is $\sim 10^2$ times higher than the mass of the largest comets, any scenario in which several comets were accreted can safely be rejected.

5.3. Relative diffusion

Alternatively, it is possible that the accreted planetesimal did not have an unusual composition and the extreme Na/Ca abundance ratio could simply be due to the different diffusion timescales of Na and Ca. In fact, for a cool helium-rich white dwarf like WD J2356–209, diffusion-accretion equilibrium cannot be assumed (Koester et al. 2011; Hollands et al. 2018). This follows from the fact that the diffusion times are of the order of a few Myr (Paquette et al. 1986; Koester 2009; Hollands et al. 2017), while the typical duration of an accretion episode is only of $10^4 - 10^6$ years (Jura 2008; Kilic et al. 2008; Melis et al. 2011; Girven et al. 2012). It is therefore possible that WD J2356–209 has stopped

accreting and that the difference between the diffusion timescales of Na and Ca has led to a composition that is not representative of the accreted planetesimal.

Once the accretion episode has stopped, relative diffusion implies that a change $\Delta \log \text{Ca/He}$ will be accompanied by a variation of the Na/Ca abundance ratio given by (Hollands et al. 2018, Equation 3),

$$\frac{\Delta \log \text{Na/Ca}}{\Delta \log \text{Ca/He}} = \frac{\tau_{\text{Ca}}}{\tau_{\text{Na}}} - 1. \quad (1)$$

In WD J2356–209, the diffusion timescale of Na is longer by a factor of ≈ 1.7 than the diffusion timescale of Ca ($\log \tau_{\text{Ca}} \approx 6.32$ and $\log \tau_{\text{Na}} \approx 6.56$).¹³ From Equation 1, it follows that every 1 dex decrease in $\log \text{Ca/He}$ is accompanied by a 0.4 increase in $\log \text{Na/Ca}$. If we assume for a moment that the accreted planetesimal had a chondritic composition with $\log \text{Na/Ca} = 0$, it implies that the Ca abundance in the atmosphere of WD J2356–209 was $\log \text{Ca/He} = -6.8$ when the accretion episode stopped, some ≈ 10 Myr ago (Kawka & Vennes 2016, Equation 4). This would raise our lower limit on the total accreted mass to $\sim 10^{23}$ g, which corresponds to the mass of a very large asteroid (Vesta has a mass of 2.6×10^{23} g, Russell et al. 2012). However, this scenario appears unlikely. Cool DZ stars are known to be much less polluted than hotter objects (Dufour et al. 2007; Koester et al. 2011; Hollands et al. 2017), possibly because the largest planetesimals are gradually scattered away from the planetary system (Veras et al. 2013, 2016; Hollands et al. 2018). In fact, according to the Montreal White Dwarf Database (Dufour et al. 2017), no known DZ star cooler than $T_{\text{eff}} = 5000$ K has a calcium abundance higher than $\log \text{Ca/He} = -9.3$.

More importantly, assuming that WD J2356–209 accreted a planetesimal with a chondritic composition might not be a realistic hypothesis. Figure 6 shows how the composition of WD J2356–209 is expected to have evolved given the diffusion timescales of Hollands et al. (2017). This evolution rules out the possibility that the accreted planetesimal had a chondrite-like composition. A more realistic hypothesis would probably be to assume that the accreted planetesimal had a sodium abundance ratio of $\log \text{Na/Ca} \approx 0.6$, which corresponds to the region where the chemical evolution track of WD J2356–209 intersects the middle of the distribution of objects plotted in Figure 6. In that case, the Ca abundance in the atmosphere of WD J2356–209 when the accretion episode stopped ≈ 4 Myr ago (i.e., $1.9\tau_{\text{Ca}}$ or $1.17\tau_{\text{Na}}$) would have been a less extreme $\log \text{Ca/He} \approx -8.3$ and the lower limit on the accreted mass is decreased to $\sim 10^{22}$ g. Assuming a typical asteroid density of 2 g cm^{-3} , the accreted planetesimal had a radius of at least 100 km.

6. CONCLUSION

We presented a detailed analysis of WD J2356–209, a very cool DZ star whose spectrum is dominated by a strong sodium feature. Thanks to our improved atmosphere models (Papers I and II), we find an excellent

fit to the photometry and the visible spectrum, allowing the first reliable atmospheric parameter determination of this object. We found that WD J2356–209 has a record sodium abundance with a number density ratio $\log \text{Na/Ca} = 1.0 \pm 0.2$.

A possible explanation for this high sodium content is that WD J2356–209 has accreted a planetesimal with an abnormally high sodium abundance and a total mass $\gtrsim 10^{21}$ g. However, we were unable to identify a solar system analog to this hypothetical planetesimal, since none of the examined candidates simultaneously matched the constraints on the sodium abundance and the total mass. Alternatively, the high sodium abundance in the atmosphere of WD J2356–209 could be explained by the slower diffusion of Na with respect to Ca. According to this scenario, the accreted object would have had a less extreme composition but a larger total mass ($\gtrsim 10^{22}$ g).

This paper concludes the observational validation of our improved cool white dwarf model atmosphere code. The excellent fit obtained for this extreme object is a clear demonstration of the capacity of our models to properly take into account the nonideal effects that prevail in the atmospheres of cool white dwarfs. In the next paper of this series, we will use our improved models to analyze a large sample of cool white dwarfs and revisit their spectral evolution.

We would like to thank Manuel Barranco for sharing with us *ab initio* potentials for the Ca–He interaction. We are grateful to the anonymous reviewer for her or his valuable comments on our manuscript. We also thank Siyi Xu for useful discussions regarding the composition of WD J2356–209.

This work was supported in part by NSERC (Canada) and the Fund FRQNT (Québec). This work has made use of the Montreal White Dwarf Database (Dufour et al. 2017).

This work has made use of data from the European Space Agency (ESA) mission *Gaia* (<https://www.cosmos.esa.int/gaia>), processed by the *Gaia* Data Processing and Analysis Consortium (DPAC, <https://www.cosmos.esa.int/web/gaia/dpac/consortium>). Funding for the DPAC has been provided by national institutions, in particular the institutions participating in the *Gaia* Multilateral Agreement.

The Pan-STARRS1 Surveys (PS1) and the PS1 public science archive have been made possible through contributions by the Institute for Astronomy, the University of Hawaii, the Pan-STARRS Project Office, the Max-Planck Society and its participating institutes, the Max Planck Institute for Astronomy, Heidelberg and the Max Planck Institute for Extraterrestrial Physics, Garching, The Johns Hopkins University, Durham University, the University of Edinburgh, the Queen’s University Belfast, the Harvard-Smithsonian Center for Astrophysics, the Las Cumbres Observatory Global Telescope Network Incorporated, the National Central University of Taiwan, the Space Telescope Science Institute, the National Aeronautics and Space Administration under Grant No. NNX08AR22G issued through the Planetary Science Division of the NASA Science Mission Directorate, the National Science Foundation Grant No.

¹³ To estimate the diffusion timescales, we use the values given by Hollands et al. (2017) for SDSS J163601.33+161907.1, as this star has similar atmospheric parameters to WD J2356–209.

AST-1238877, the University of Maryland, Eotvos Lorand University (ELTE), the Los Alamos National Laboratory, and the Gordon and Betty Moore Foundation.

This publication makes use of data products from the Wide-field Infrared Survey Explorer, which is a joint

project of the University of California, Los Angeles, and the Jet Propulsion Laboratory/California Institute of Technology, funded by the National Aeronautics and Space Administration.

REFERENCES

- Abel, M., Frommhold, L., Li, X., & Hunt, K. L. 2012, *J. Chem. Phys.*, 136, 044319
- Allard, N., Royer, A., Kielkopf, J., & Feautrier, N. 1999, *Phys. Rev. A*, 60, 1021
- Allard, N. F., & Alekseev, V. A. 2014, *Advances in Space Research*, 54, 1248
- Allard, N. F., Allard, F., Hauschildt, P. H., Kielkopf, J. F., & Machin, L. 2003, *A&A*, 411, L473
- Allard, N. F., Homeier, D., Guillon, G., Viel, A., & Kielkopf, J. 2014, *Journal of Physics: Conference Series*, 548, 012006
- Allard, N. F., Kielkopf, J. F., Blouin, S., et al. 2018, *A&A*, 619, A152
- Allard, N. F., Leininger, T., Gadéa, F. X., Brousseau-Couture, V., & Dufour, P. 2016, *A&A*, 588, A142
- Bardyn, A., Baklouti, D., Cottin, H., et al. 2017, *MNRAS*, 469, S712
- Baron, E., & Hauschildt, P. H. 1998, *ApJ*, 495, 370
- Becker, A., Lorenzen, W., Fortney, J. J., et al. 2014, *ApJS*, 215, 21
- Bergeron, P. 2003, *ApJ*, 586, 201
- Bergeron, P., Ruiz, M. T., Hamuy, M., et al. 2005, *ApJ*, 625, 838
- Bergeron, P., Ruiz, M. T., & Leggett, S. K. 1997, *ApJS*, 108, 339
- Blouin, S., Dufour, P., & Allard, N. F. 2018a, *ApJ*, 863, 184
- Blouin, S., Dufour, P., Allard, N. F., & Kilic, M. 2018b, *ApJ*, 867, 161
- Blouin, S., Kowalski, P. M., & Dufour, P. 2017, *ApJ*, 848, 36
- Chambers, K. C., Magnier, E. A., Metcalfe, N., et al. 2016, *ArXiv e-prints*, arXiv:1612.05560
- Croll, B., Dalba, P. A., Vanderburg, A., et al. 2017, *ApJ*, 836, 82
- Dufour, P., Bergeron, P., Schmidt, G. D., et al. 2006, *ApJ*, 651, 1112
- Dufour, P., Blouin, S., Coutu, S., et al. 2017, in *Astronomical Society of the Pacific Conference Series*, Vol. 509, 20th European White Dwarf Workshop, ed. P.-E. Tremblay, B. Gänsicke, & T. Marsh, 3
- Dufour, P., Kilic, M., Fontaine, G., et al. 2012, *ApJ*, 749, 6
- Dufour, P., Bergeron, P., Liebert, J., et al. 2007, *ApJ*, 663, 1291
- Farihi, J., Barstow, M. A., Redfield, S., Dufour, P., & Hambly, N. C. 2010, *MNRAS*, 404, 2123
- Farihi, J., Dufour, P., Napiwotzki, R., & Koester, D. 2011, *MNRAS*, 413, 2559
- Farihi, J., Gänsicke, B. T., & Koester, D. 2013, *Science*, 342, 218
- Farihi, J., Jura, M., & Zuckerman, B. 2009, *ApJ*, 694, 805
- Fontaine, G., Brassard, P., & Bergeron, P. 2001, *PASP*, 113, 409
- Gaia Collaboration. 2016, *A&A*, 595, A1
- . 2018, *A&A*, 616, A1
- Gänsicke, B. T., Marsh, T. R., Southworth, J., & Rebassa-Mansergas, A. 2006, *Science*, 314, 1908
- Gänsicke, B. T., Aungwerojwit, A., Marsh, T. R., et al. 2016, *ApJ*, 818, L7
- GharibNezhad, E., Shayesteh, A., & Bernath, P. F. 2013, *MNRAS*, 432, 2043
- Giammichele, N., Bergeron, P., & Dufour, P. 2012, *ApJS*, 199, 29
- Irwin, J., Brinkworth, C. S., Farihi, J., et al. 2012, *ApJ*, 749, 154
- Harris, H. C., Liebert, J., Kleinman, S. J., et al. 2003, *AJ*, 126, 1023
- Harrison, J. H. D., Bonsor, A., & Madhusudhan, N. 2018, *MNRAS*, 479, 3814
- Hauschildt, P. H., & Baron, E. 1999, *Journal of Computational and Applied Mathematics*, 109, 41
- Hauschildt, P. H., Baron, E., & Allard, F. 1997, *ApJ*, 483, 390
- Hernando, A., Barranco, M., Mayol, R., Pi, M., & Krośnicki, M. 2008, *Phys. Rev. B*, 77, 024513
- Hollands, M. A., Gänsicke, B. T., & Koester, D. 2018, *MNRAS*, 477, 93
- Hollands, M. A., Koester, D., Alekseev, V., Herbert, E. L., & Gänsicke, B. T. 2017, *MNRAS*, 467, 4970
- Homeier, D., Allard, N., Allard, F., et al. 2005, in *Astronomical Society of the Pacific Conference Series*, Vol. 334, 14th European Workshop on White Dwarfs, ed. D. Koester & S. Moehler, 209
- Homeier, D., Allard, N., Johnas, C. M. S., Hauschildt, P. H., & Allard, F. 2007, in *Astronomical Society of the Pacific Conference Series*, Vol. 372, 15th European Workshop on White Dwarfs, ed. R. Napiwotzki & M. R. Burleigh, 277
- Jessberger, E. K., Christoforidis, A., & Kissel, J. 1988, *Nature*, 332, 691
- Jørgensen, U. G., Hammer, D., Borysow, A., & Falckegaard, J. 2000, *A&A*, 361, 283
- Jura, M. 2003, *ApJ*, 584, L91
- . 2008, *AJ*, 135, 1785
- Jura, M., & Young, E. D. 2014, *Annual Review of Earth and Planetary Sciences*, 42, 45
- Kawka, A., & Vennes, S. 2016, *MNRAS*, 458, 325
- Kilic, M., Farihi, J., Nitta, A., & Leggett, S. K. 2008, *AJ*, 136, 111
- Kissel, J., Altwegg, K., Clark, B. C., et al. 2007, *Space Sci. Rev.*, 128, 823
- Koester, D. 2009, *A&A*, 498, 517
- Koester, D., Girven, J., Gänsicke, B. T., & Dufour, P. 2011, *A&A*, 530, A114
- Kowalski, P. M., Mazevet, S., Saumon, D., & Challacombe, M. 2007, *Phys. Rev. B*, 76, 075112
- Lodders, K. 2003, *ApJ*, 591, 1220
- McCook, G. P., & Sion, E. M. 1999, *ApJS*, 121, 1
- Melis, C., & Dufour, P. 2017, *ApJ*, 834, 1
- Melis, C., Farihi, J., Dufour, P., et al. 2011, *ApJ*, 732, 90
- Melis, C., Jura, M., Albert, L., Klein, B., & Zuckerman, B. 2010, *ApJ*, 722, 1078
- Oke, J. B., Cohen, J. G., Carr, M., et al. 1995, *PASP*, 107, 375
- Oppenheimer, B. R., Hambly, N. C., Digby, A. P., Hodgkin, S. T., & Saumon, D. 2001, *Science*, 292, 698
- Paquette, C., Pelletier, C., Fontaine, G., & Michaud, G. 1986, *ApJS*, 61, 197
- Pätzold, M., Andert, T., Hahn, M., et al. 2016, *Nature*, 530, 63
- Raddi, R., Gänsicke, B. T., Koester, D., et al. 2015, *MNRAS*, 450, 2083
- Rocchetto, M., Farihi, J., Gänsicke, B. T., & Bergfors, C. 2015, *MNRAS*, 449, 574
- Rolland, B., Bergeron, P., & Fontaine, G. 2018, *ApJ*, 857, 56
- Rumble, J. R. 2018, *CRC Handbook of Chemistry and Physics*, 99th edn. (Boca Raton, FL: CRC Press/Taylor & Francis)
- Russell, C. T., Raymond, C. A., Coradini, A., et al. 2012, *Science*, 336, 684
- Salim, S., Rich, R. M., Hansen, B. M., et al. 2004, *ApJ*, 601, 1075
- Saumon, D., Chabrier, G., & van Horn, H. M. 1995, *ApJS*, 99, 713
- Shayesteh, A., Ram, R. S., & Bernath, P. F. 2013, *Journal of Molecular Spectroscopy*, 288, 46
- Tennyson, J., & Yurchenko, S. N. 2012, *MNRAS*, 425, 21
- Tennyson, J., Yurchenko, S. N., Al-Refaie, A. F., et al. 2016, *Journal of Molecular Spectroscopy*, 327, 73
- Vanderburg, A., Johnson, J. A., Rappaport, S., et al. 2015, *Nature*, 526, 546
- Veras, D., Mustill, A. J., Bonsor, A., & Wyatt, M. C. 2013, *MNRAS*, 431, 1686
- Veras, D., Mustill, A. J., Gänsicke, B. T., et al. 2016, *MNRAS*, 458, 3942
- Wang, H. S., Lineweaver, C. H., & Ireland, T. R. 2018, *Icarus*, 299, 460
- Weck, P. F., Stancil, P. C., & Kirby, K. 2003, *J. Chem. Phys.*, 118, 9997
- Weissman, P. R. 2007, in *IAU Symposium*, Vol. 236, Near Earth Objects, our Celestial Neighbors: Opportunity and Risk, ed. G. B. Valsecchi, D. Vokrouhlický, & A. Milani, 441–450
- Wright, E. L., Eisenhardt, P. R. M., Mainzer, A. K., et al. 2010, *AJ*, 140, 1868
- Xu, S., Zuckerman, B., Dufour, P., et al. 2017, *ApJ*, 836, L7
- Zuckerman, B., & Becklin, E. E. 1987, *Nature*, 330, 138
- Zuckerman, B., Koester, D., Dufour, P., et al. 2011, *ApJ*, 739, 101
- Zuckerman, B., Koester, D., Melis, C., Hansen, B. M., & Jura, M. 2007, *ApJ*, 671, 872